

Structural characterization of submerged granular packingsZ. M. Jakšić,¹ J. R. Šćepanović,¹ I. Lončarević,² Lj. Budinski-Petković,² S. B. Vrhovac,^{1,*} and A. Belić¹¹*Institute of Physics Belgrade, University of Belgrade, Pregrevica 118, Zemun 11080, Belgrade, Serbia*²*Faculty of Engineering, Trg D. Obradovića 6, Novi Sad 21000, Serbia*

(Received 14 May 2014; revised manuscript received 16 November 2014; published 30 December 2014)

We consider the impact of the effective gravitational acceleration on microstructural properties of granular packings through experimental studies of spherical granular materials saturated within fluids of varying density. We characterize the local organization of spheres in terms of contact connectivity, distribution of the Delaunay free volumes, and the shape factor (parameter of nonsphericity) of the Voronoï polygons. The shape factor gives a clear physical picture of the competition between less and more ordered domains of particles in experimentally obtained packings. As the effective gravity increases, the probability distribution of the shape factor becomes narrower and more localized around the lowest values of the shape factor corresponding to regular hexagon. It is found that curves of the pore distributions are asymmetric with a long tail on the right-hand side, which progressively reduces while the effective gravity gets stronger for lower densities of interstitial fluid. We show that the distribution of local areas (Voronoi cells) broadens with decreasing value of the effective gravity due to the formation of loose structures such as large pores and chainlike structures (arches or bridges). Our results should be particularly helpful in testing the newly developed simulation techniques involving liquid-related forces associated with immersed granular particles.

DOI: [10.1103/PhysRevE.90.062208](https://doi.org/10.1103/PhysRevE.90.062208)

PACS number(s): 81.05.Rm, 45.70.Cc, 83.80.Fg

I. INTRODUCTION

The packing of classical particles that interact only through contact forces is one of the enduring problems in physics. Dense packings of hard spheres are an important starting point for the study of simple liquids, glasses, colloids, and granular matter [1–3]. Considerable work has been done in the past on dry granular piles, both theoretically and experimentally, exploring the influence of the microstructural arrangement of the grains on the macroscopic properties of the packing. In the 1960s, Bernal studied the arrangement for 500–1000 particles taken from the interior of an amorphous packing with 5000 particles [4,5]. In more recent times, Aste *et al.* used x-ray tomography to study several different packings containing almost 10^5 grains [6,7]. Slotterback *et al.* analyzed the position of 16 000 spheres by using the index-matching fluid and laser-scattering-based imaging method to find position of the particles [8]. These experiments provide useful data for studying the microstructural properties of granular packings, such as radial distribution function, number of neighbors, orientation order metric, pore-size distributions, etc.

Most experiments so far have been performed in dry systems where the interstitial medium is air. A considerably smaller number of experiments deal with granulates completely immersed in a less dense liquid. Usually, the objective of these studies has been the analysis of the effects of interstitial fluid on the segregation and mixing dynamics in a rotating drum [9–13]. In some experiments, the replacement of air with a liquid has been used as a strategy for obtaining the reduced gravity conditions (the effect of buoyancy may be taken care of by rescaling the gravity). Onoda and Liniger [14] determined the random loose packing of uniform glass spheres at the limit of zero gravitational force. Costantino *et al.* [15] analyzed

the dependence of the low-velocity drag force in a granular material on the effective gravitational acceleration. In both experiments the spherical granular materials were submerged within liquids of varying density.

The present work is focused on two-dimensional (2D) disordered granular packings formed in liquids. Fluid density is varied by using different solutions of zinc chloride (ZnCl_2) and water. The experiment is designed to investigate the arrangement of grains. Our aim is to characterize the structure of disordered disk packings and to quantify the structural changes associated with different intensities of effective gravity. Analysis at the microscopic scale is based on the Voronoï tessellation. Voronoï tessellation divides a two-dimensional region occupied by grains into space filling, nonoverlapping convex polygons. We apply the concept of shape factor, introduced by Moucka and Nezbeda [16], for tracking the changes in the structure as a liquidlike system approaches a disordered jammed state. This quantity was recently used to study the crystallization of two-dimensional systems, both in simulation [16] and experiment [17]. Shape factor is a dimensionless measure of deviation of the Voronoï cells from circularity. Distribution of the shape factor clearly indicates the presence of different underlying substructures (domains) in the packing.

The volume distribution and shape characteristics of the interstitial voids are important parameters in describing and evaluating the structural properties of granular packings. Next, we compute the distributions of the Voronoï cell volume, which describe the deviation of 2D packings of spheres from a regular hexagonal arrangement [18]. Finally, the Delaunay triangulation is used to quantify the volume distribution of pores of our particle packings [6,19,20].

The following section describes the various components of the apparatus and summarizes the most important features and technical details that are relevant to our experimental procedures. The experimental results are reported and discussed in Sec. III. In the last section, we draw some conclusions.

*vrhovac@ipb.ac.rs; <http://www.ipb.ac.rs/~vrhovac/>

II. EXPERIMENTAL SETUP AND PROCEDURES

Now we describe in more detail a conceptually simple experiment aimed at understanding the relation between reduced gravity conditions and local structure of granular packings. The experiments were conducted in a glass rectangular tank with base dimensions of 480 mm × 200 mm and a depth of 590 mm. The tank was entirely filled with various solutions of zinc chloride (ZnCl₂) and water, which allowed the density of the mixture to be controlled. We examined the two-dimensional (2D) submerged random packings of monodisperse acrylic spheres with diameter d_s of 6.00 ± 0.01 mm and mass $m_1 = 0.20$ g (King Arms Airsoft Accessories). A 470 × 500 mm glass plate was used as the removable confining wall for the experiment. It was mounted inside of the vessel, parallel to the front wall of the container. These two parallel glass plates form a thin cell with an inner gap of thickness $\Delta l = 6.4$ mm, slightly larger than the diameter of the spheres d_s . A sketch of the experimental setup is shown in Fig. 1.

The two layers of spheres were initially submerged and held in place near the top of the tank by means of a horizontal plexiglass plate. The plate was covered with a sandpaper of large roughness by which the layers of particles were randomized. The platform was placed beneath the surface of the liquid, along the top edge of the confining wall. The level of the liquid was always kept $\approx 3\text{--}5$ cm above the top of the grains, so that our results were not affected by capillary forces. The angle of the platform is then slowly increased up to an angle $\theta = 7.5^\circ$, thereby inducing a single avalanche. After the plane rotation, grains therefore freely slide downward and fall through the liquid into quasi-two-dimensional rectangular box in which they reach a mechanically stable state. The system was also initialized by pouring grains near the top

of the inclined plane (the case of intermittent series of avalanches). In the both cases the final packing was obtained by random rain of beads under gravity. We have verified that usage of different preparation procedures gives quantitatively very similar structural characteristics for submerged granular packings, but we opted for the single avalanche one. It must be emphasized that our method of preparation ensures the formation of complex patterns and cooperative structures such as arches or bridges in all parts of the final packing. An arch or a bridge is a cooperative structure that is stable thanks to the contributions of every particle in it. These multiparticle structures are seen to naturally emerge when a granular system locally solidifies due to the dissipation [21–25].

The microstructural properties of immersed packings were studied in liquid whose density could be varied. An aqueous solution of zinc chloride (ZnCl₂) was used because it is very soluble in water (4320 g/L at 25 °C). It is well known that ZnCl₂ is corrosive to metals and therefore experimental apparatus did not contain any metal parts. The spheres density was $\rho_1 = 1.80$ g/cm³ and the density of liquid ρ_0 could be adjusted to include neutrally buoyant conditions, $\rho_0 \approx \rho_1$. However, the highest density of the liquid in which the granular packings were formed had a slightly lower value of $\rho_0 = 1.70$ g/cm³. The density of the liquid was adjusted to lower densities by decreasing the concentration of ZnCl₂, so that the effective gravitational force on the spheres could be varied. Actually, the liquid buoyant force effectively reduced the acceleration owing to gravity, resulting in an effective gravitational acceleration of $g_{\text{eff}}^{(1)} = g(\rho_1 - \rho_0)/\rho_1$, where $g = 9.81$ m/s² is the Earth’s gravity. The physical properties of different aqueous solutions of ZnCl₂ used in the experiments are summarized in Table I. We were able to increase the fluid density to a range of values between the density of water and the density of grains [we label our solutions as (A)–(F) in Table I]. Our maximum density was $\rho_0 = 1.70$ g/cm³, giving us a range in the effective gravitational acceleration from $g_{\text{eff}}^{(1)}(\text{F}) = 4.36$ m/s² in water down to $g_{\text{eff}}^{(1)}(\text{A}) = 5.46 \times 10^{-1}$ m/s² in the solution of type (A). In the last column of Table I values of the effective gravity g_{eff} normalized by g are given for the used liquids.

The problem with our approach is that during the settlement of the packing the dynamics of spheres depends on the fluid viscosity η . The maximum viscosity of our liquids was for the highest density solution and its value was $\eta \lesssim 6.5$ mPas (see Table I). It is obvious that larger buoyant force combined

TABLE I. Table summarizes the values of density ρ_0 and viscosity η of aqueous solutions of zinc chloride (ZnCl₂) at $21.0 \pm 0.5^\circ\text{C}$ [37]. We label our solutions as (A)–(F). The values of the effective gravity $g_{\text{eff}}^{(1)}$ normalized by g and the mean packing fraction $\langle \rho \rangle$ are given in the two last columns, respectively.

Aqueous solution of ZnCl ₂	ρ_0 (g/cm ³)	η (mPa s)	$g_{\text{eff}}^{(1)}/g$	$\langle \rho \rangle$
(A)	1.70	6.5	5.57×10^{-2}	0.812
(B)	1.60	4.3	1.11×10^{-1}	0.829
(C)	1.50	2.5	1.67×10^{-1}	0.846
(D)	1.40	2.0	2.22×10^{-1}	0.863
(E)	1.30	1.7	2.78×10^{-1}	0.871
(F)	1.00	1.0	4.44×10^{-1}	0.876

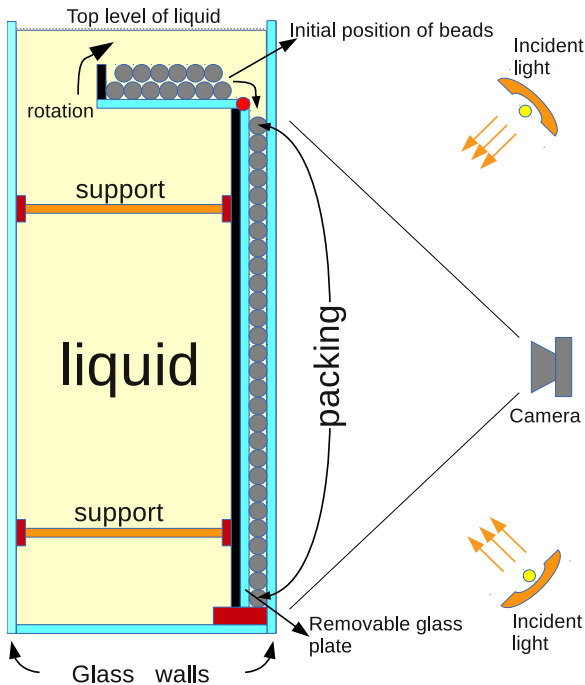


FIG. 1. (Color online) Schematic drawing of the experimental setup.

with viscous force will slow the settlement of the packing. Therefore, experiments were also carried out with spheres of mass $m_2 = 0.12 \text{ g} < m_1$ and diameter $d_s = 6.00 \pm 0.01 \text{ mm}$ ($\rho_2 = 1.06 \text{ g/cm}^3 < \rho_1$). The cell was filled with water of density 1000 kg/m^3 and viscosity 1 mPas , so that the normalized effective gravity $g_{\text{eff}}^{(2)}/g$ for immersed beads was of 5.75×10^{-2} . The values of the normalized effective gravities $g_{\text{eff}}^{(1)(A)}/g$ and $g_{\text{eff}}^{(2)}/g$ are close to each other, while the solution (A) is 6.5 times more viscous than water. As evidenced below, we find that the microstructural properties of immersed granular packings are similar in both cases, suggesting that viscous effects on grain motion had little impact on the formation of complex structural components in static granular pack. It must be stressed that we chose millimetric beads that were coarse enough for interparticle forces (e.g., van der Waals force) to be negligible compared with inertial forces, so that aggregation effects are not present.

Experimental study of microstructural properties of granular packings requires a precise measurement of grain positions. For this reason, a digital camera (Canon SX10 IS) is used to capture high-resolution images ($3648 \times 2736 \text{ pixel}^2$ spatial resolution) of whole packings. The camera is firmly fixed to the plane 72 cm away from the planar packing with its optical axis perpendicular to it. Fluorescent lamps located beside the camera provide diffuse lighting and a black cloth isolates the experimental device from the ambient light. Figures 2(a) and 2(b) show high-resolution images of typical packings formed in solutions (E) and (A), respectively (see Table I). If we compare the two snapshots taken from the central parts of packings, the structure of clusters and pores appear quite different to the eye. We clearly observe the correlation between the degree of disorder in the system of grains and the value of solution density. The center of each grain is accurately determined using the image-processing program based on the Standard Hough Transform (SHT) [26]. This involves the measurement of the coordinates and diameters of 5000–6000 particles. In the output bitmap image, the diameters of grains are ≈ 40 pixels. This analysis allows one to detect the centers of spheres with resolution of 0.15 mm , i.e., centers are located to within $0.025d_s$.

It should be noted that we control the ambient temperature of the laboratory. Our laboratory is kept at $21.0 \pm 0.5^\circ \text{C}$ when the experiments are performed.

III. EXPERIMENTAL RESULTS AND DISCUSSION

Here we try to compare quantitatively the structural characteristics of packings corresponding to different intensities of the effective gravity $g_{\text{eff}}^{(1)}/g = (\rho_1 - \rho_0)/\rho_1$. In order to gain a basic insight into the microstructure of the packings generated in the experiments, we first consider the radial distribution function $g(r)$ (or pair-correlation function), which gives information about the long-range interparticle correlations and their organization [27]. Figure 3 shows $g(r)$ functions for the various packings studied here. The presence of peaks after the peak at $r = d_s$ (associated with spheres in contact) is a clear indication that the packings are organized, i.e., characteristic structures with distinct local patterns are present. For all the packings, there is a pronounced splitting of the second peak

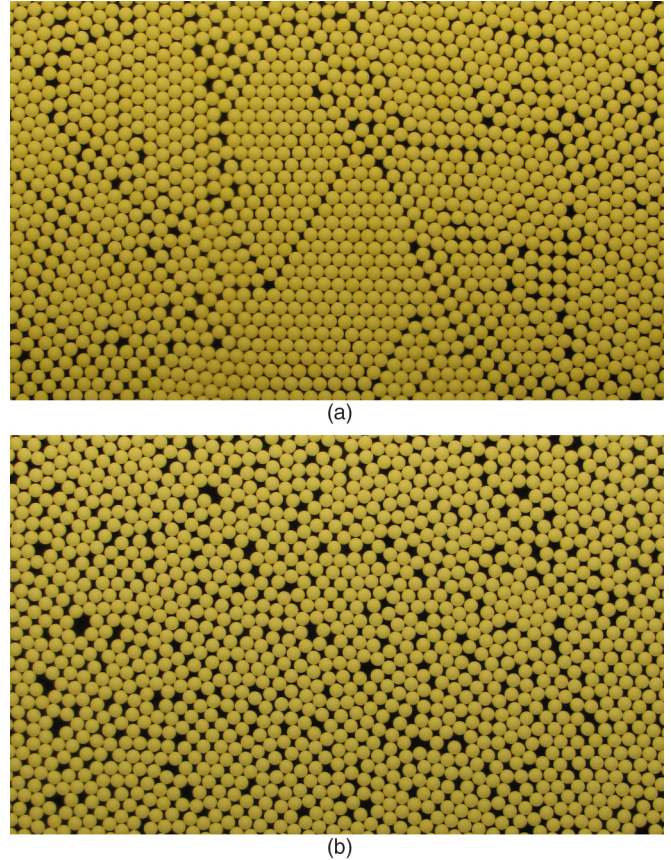


FIG. 2. (Color online) Sample images of immersed beads observed in aqueous solution of zinc chloride (ZnCl_2): (a) solution of type (E), and (b) solution of type (A) (see Table I). Two snapshots are taken from the central part of the packings.

in $g(r)$ into two subpeaks, located at $r = \sqrt{3}$ and 2 . Such a splitting of the second peak has long been known [7,28–30]; it is a clear signature of the strong local order in the first two coordination shells of the packing. It is easy to verify that a radial distance $r/d_s \approx \sqrt{3}$ is consistent with configurations in two dimensions made by placing the centers of four spheres on the vertices of two equilateral triangles (with edge length d_s), which share an edge, whereas the peak at $r/d_s \approx 2$ is due to three or more spheres, which are lying along a straight line. In other words, the separation $r = 2d_s$ corresponds to the largest distance that can separate two spheres that have one common neighbor. The separation $r = \sqrt{3}d_s$ corresponds to the largest possible separation between two particles that have two common neighbors. Furthermore, Fig. 3 shows that the two peaks at $r/d_s \approx \sqrt{3}$ and $r/d_s \approx 2$ both increase in height with packing density ρ . The growth with density ρ is faster in the peak at $r = \sqrt{3}d_s$ with respect to that in the peak at $r = 2d_s$. This indicates an increasing organization in the packing structure. For packings formed in dense solutions, such as solutions (A), (B), and (C), such a local organization is limited to very short distances yielding globally nonordered packings [see, e.g., Fig. 2(b)]. For packings formed in less dense solutions (D), (E), and (F) peaks are clearly observed near d_s , $\sqrt{3}d_s$, $2d_s$, $\sqrt{7}d_s$, $3d_s$, $2\sqrt{3}d_s$, and $\sqrt{13}d_s$, indicating a hexagonal packing. At large distances, the peaks broaden,

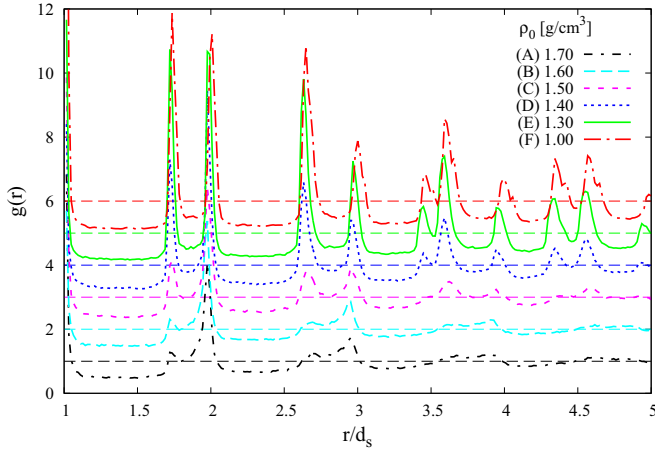


FIG. 3. (Color online) Radial distribution function $g(r)$ as a function of separation r/d_s . From bottom to top results are shown for packings formed in aqueous solutions (A)–(F) of ZnCl_2 . Plots are evenly shifted vertically for clarity. The values of the mean packing fraction $\langle\rho\rangle$ for the corresponding packings are given in the Table I.

merge with one another, and become lost in the continuum background $g(r) \rightarrow 1$.

In order to analyze the granular organization at the microscopic scale, we calculate the number of neighbors for each grain and analyze the disposition of the particles as nodes of the contact network. The coordination number, i.e., the average number of disks in contact with a given disk is frequently investigated parameter in the literature on granular packings [6,7]. It varies with the definition of contact, i.e., the minimal or cutoff distance d_c between two disks below which they are regarded to be in contact. The coordination number is very sensitive to the changes of cutoff distance d_c . Figure 4 shows the mean coordination numbers $\langle N_c \rangle$ for

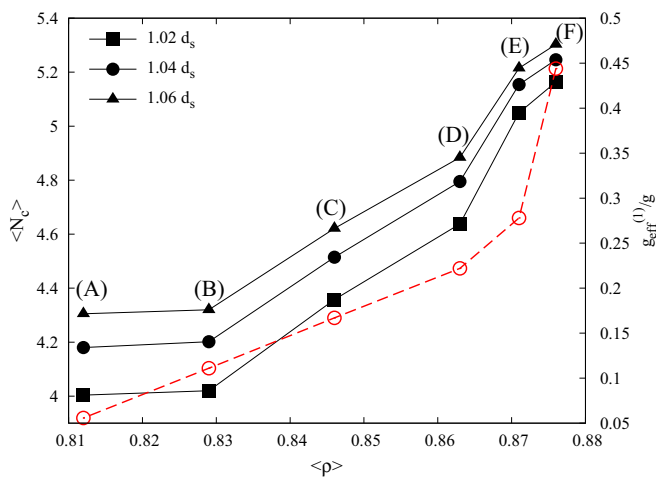


FIG. 4. (Color online) Values of the mean coordination number $\langle N_c \rangle$ for packings formed in aqueous solutions (A)–(F) of ZnCl_2 (see Table I). Results are given for three values of the cutoff parameter $d_c = 1.02d_s$ (squares), $1.04d_s$ (circles), and $1.06d_s$ (triangles). The values of the effective gravity $g_{\text{eff}}^{(1)}$ normalized by g (red open circles) are given on the right axis. The values of the mean packing fraction $\langle\rho\rangle$ for the corresponding packings are given on the x axis.

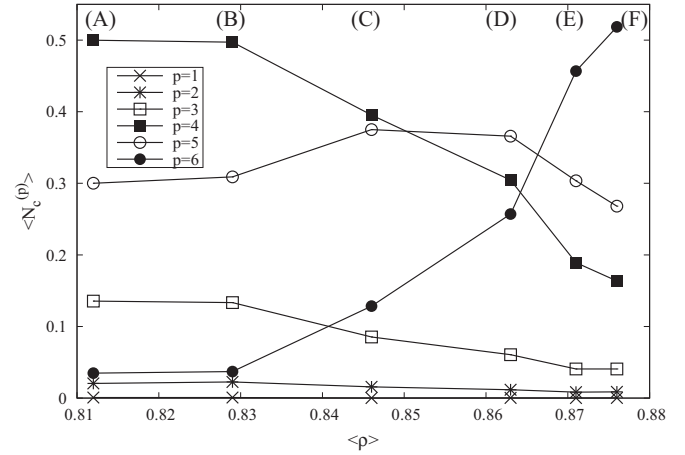


FIG. 5. Connectivity numbers $\langle N_c^{(p)} \rangle$ ($p = 1, \dots, 6$) calculated for packings formed in aqueous solutions (A)–(F) of ZnCl_2 (see Table I). The cutoff distance d_c is $1.04d_s$. The values of the mean packing fraction $\langle\rho\rangle$ are given on the x axis. The corresponding values of normalized effective gravity $g_{\text{eff}}^{(1)}/g$ are given in the Fig. 4.

packings formed in aqueous solutions (A)–(F) of ZnCl_2 (see Table I). Results are given for three different cutoff distances: $d_c = 1.02d_s$, $1.04d_s$, and $1.06d_s$. In all cases, $\langle N_c \rangle$ increases with density $\langle\rho\rangle$ of packings and ranges between 4.0 and 5.3 depending on the threshold distance d_c and on the sample density $\langle\rho\rangle$. Let us remark that the choice of such threshold d_c is not critical. The properties reported in this paper are consistently observed in a range of thresholds from 1.02–1.06. Because of that, in the present work we choose a threshold distance of 1.04 sphere diameter d_s .

Due to dynamic rearrangements in the packing, the number of contact neighbors p varies from particle to particle. In a two-dimensional bed of convex particles, p can vary from 1–6. The connectivity disorder of a packing can be characterized by the fraction $\langle N_c^{(p)} \rangle$ of disks having p contact neighbors. $\langle N_c^{(1)} \rangle$ corresponds to dead ends of particle chains. $\langle N_c^{(2)} \rangle$ and $\langle N_c^{(3)} \rangle$ are related to chaining and branching, respectively. $\langle N_c^{(4)} \rangle$ corresponds to a situation where a particle is supported by two underlying grains and supports two others (piling). $\langle N_c^{(5)} \rangle$ and $\langle N_c^{(6)} \rangle$ correspond to jammed and ordered configurations.

Figure 5 shows the variation of the connectivity numbers $\langle N_c^{(p)} \rangle$, $p = 1, \dots, 6$ with density of packings $\langle\rho\rangle$ formed in aqueous solutions (A)–(F) of ZnCl_2 (Table I). All connectivity numbers, except $\langle N_c^{(5)} \rangle$, vary monotonically with packing fraction $\langle\rho\rangle$. Up to $\langle\rho\rangle$ (C) = 0.846, $\langle N_c^{(5)} \rangle$ and $\langle N_c^{(6)} \rangle$ increase at the expense of $\langle N_c^{(2)} \rangle$, $\langle N_c^{(3)} \rangle$, and $\langle N_c^{(4)} \rangle$ which decrease. After $\langle\rho\rangle$ (D) = 0.863, $\langle N_c^{(6)} \rangle$ increases more rapidly, so that $\langle N_c^{(5)} \rangle$ starts to slightly decrease. $\langle N_c^{(1)} \rangle$ remains rather constant in the whole range of densities. The lowest densities $\langle\rho\rangle = 0.81$ –0.83 correspond to the packings characterized by piling (i.e., $\langle N_c^{(4)} \rangle$ is the largest connectivity number). Chaining ($\langle N_c^{(2)} \rangle$) and branching ($\langle N_c^{(3)} \rangle$) are also important characteristics of these packings. Values of $\langle N_c^{(2)} \rangle$ (chaining) and $\langle N_c^{(3)} \rangle$ (branching) suggest the presence of bridges (or arches) [21,24,25]. While the effective gravity $g_{\text{eff}}^{(1)}/g$ gets stronger for lower densities of the solution [(C)–(F)], the first effect is that the particles tend to increase the fraction of the

packing composed of dense ordered domains. Consequently, connectivity number $\langle N_c^{(6)} \rangle$ increases rapidly, and the system becomes more compact. Simultaneously, piling $\langle N_c^{(4)} \rangle$, branching $\langle N_c^{(3)} \rangle$, and chaining $\langle N_c^{(2)} \rangle$ decrease. The qualitatively same results are obtained for different values of the threshold distance in a range between $d_c = 1.02d_s$ and $1.06d_s$.

Further analysis is based on the Voronoi tessellation, which allows us to unambiguously decompose any arbitrary arrangement of spheres into a space-filling set of cells. The packings are analyzed in terms of volume distributions of the pores and distributions of the shape factor. The Voronoi tessellation is one of the simplest mathematical models of a cellular structure. Given a set \mathcal{A} of discrete points in the plane π , for almost any point $x \in \pi$ in the plane π there is one specific point $a_i \in \mathcal{A}$, which is closest to x . The set of all points of the plane, which are closer to a given point $a_i \in \mathcal{A}$ than to any other point $a_j \neq a_i$, $a_j \in \mathcal{A}$, is the interior of a convex polygon \mathcal{P}_i usually called the Voronoi cell of a_i . The set of the polygons $\{\mathcal{P}_i\}$, each corresponding to (and containing) one point $a_i \in \mathcal{A}$, is the Voronoi tessellation corresponding to \mathcal{A} , and provides a partitioning of the plane π . In this work, the QUICKHULL algorithm [31] is used to compute the Voronoi diagrams in MATLAB[®] for a given set of spheres on a plane.

Voronoi cells are convex and their edges join at trivalent vertices, i.e., each vertex is equidistant to three neighboring disks. Two disks sharing a common cell edge are neighbors. As suggested by Bideau and coworkers [32,33], a pore in 2D packing can be defined as a virtual circle centered on the vertex and in contact with the three neighboring disks. The second convenient definition of a pore is based on the Delaunay triangulation (DT), which is a natural way to subdivide a 2D packing structure into a system of triangles with vertices on the centers of neighboring disks. Consequently, the circle circumscribed about a Delaunay triangle has its center at the vertex of a Voronoi polygon. In this study we define the pore as a part of the Delaunay triangle not occupied by the disks (Delaunay free volume) [6,20]. The pore volume v is normalized by the volume of the grains, $v_s = d_s^2\pi/4$.

Here we consider the probability distribution $P(v)$ of the Delaunay free volume v . The distribution function $P(v)$ is related to the probability of finding a pore with volume v . It is normalized to unity, namely, $\int_0^\infty dv P(v) = 1$. Fluctuations in the measurements of $P(v)$ are reduced by averaging over six different experiments, performed under the same conditions. We compare volume distribution of the pores $P(v)$ for packings corresponding to different intensities of the effective gravity $g_{\text{eff}}^{(1)}$, as reported in Fig. 6. Here, the pore distributions $P(v)$ obtained for packings formed in aqueous solutions of zinc chloride (A)–(F) have been plotted; their mean packing fractions $\langle \rho \rangle$ are, respectively, 0.812, 0.829, 0.846, 0.863, 0.871, and 0.876 (see also Table I). It can be seen that these distribution functions are dependent on the solution density ρ_0 . The curves of volume distribution $P(v)$ are asymmetric with a quite long tail on the right-hand side, which progressively reduces while the effective gravity $g_{\text{eff}}^{(1)}$ gets stronger for lower densities of solution. We observe the appearance of two peaks of $P(v)$ on fixed positions, approximately at 0.05 and 0.13. It is easy to understand which kind of local configuration contributes most to each peak of the $P(v)$. The Delaunay cells with free dimensionless volume $\sqrt{3}/\pi - 1/2 \approx 0.051$

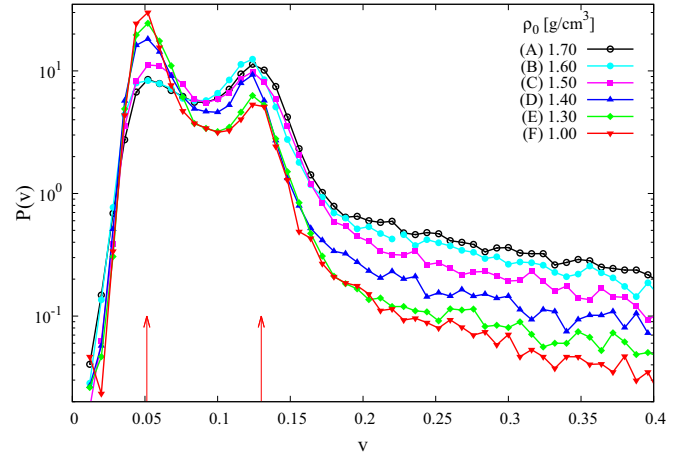


FIG. 6. (Color online) Volume distribution of the pores $P(v)$ for packings formed in aqueous solutions (A)–(F) of ZnCl_2 (see Table I). The pore volume v is normalized by the volume of the grains, $v_d = d_s^2\pi/4$. Vertical arrows are at the volumes $\sqrt{3}/\pi - 1/2$ and $2/\pi - 1/2$. As the density of solutions ρ_0 decreases, the tail of the distribution corresponding to the largest pores is being reduced.

correspond to the local arrangements of hexagonal symmetry, when three disks are all in touch with each other with centers on the vertices of a unilateral triangle. The cells with free volume $2/\pi - 1/2 \approx 0.13$ correspond to the local configurations of quadratic symmetry, when four disks are all in touch with each other with centers on the vertices of a square. Actually, such local organization in two dimensions corresponds to piling, i.e., a natural situation where a disk is supported by two underlying disks and supports two others. Therefore, the behavior of the two peaks of distribution $P(v)$ should be in accordance with changes of connectivity numbers $\langle N_c^{(6)} \rangle$ and $\langle N_c^{(4)} \rangle$. Indeed, Figs. 5 and 6 suggests that the decrease of $\langle N_c^{(4)} \rangle$ is accompanied by decrease of the height of the second peak of distribution $P(v)$. Simultaneously, increase of $\langle N_c^{(6)} \rangle$ is accompanied by an increase of the height of the first peak of $P(v)$. Furthermore, we have verified that other choices for the elementary volumes, such as the void volume proposed by Bideau and coworkers [32,33], do not yield to such a neat second peak in the volume distribution.

Further, we investigate the correlation between the degree of disorder in the system of grains and the values of the effective gravity g_{eff}/g . For this purpose we use the concept of the shape factor to measure the topology of the Voronoi cells. The shape factor ζ (parameter of nonsphericity) combines the circumference C and the surface S of the Voronoi cells [16,34]. It is defined as

$$\zeta = \frac{C^2}{4\pi S}. \quad (1)$$

For a square $\zeta = 4/\pi \approx 1.273$, for a regular pentagon $\zeta = \pi/5 \tan(\pi/5) \approx 1.156$, and for a regular hexagon $\zeta = 6/\sqrt{3}\pi^2 \approx 1.103$. Generally, for a regular N -sided polygon we have $\zeta = (N/\pi) \tan(\pi/N)$, which sets a lower bound for other N -sided polygons. Thus a circular structure has a shape factor $\zeta = 1$, while for a convex polygon, the more anisotropic is the polygon, the higher is $\zeta > 1$.

TABLE II. Table summarizes the classification of the Voronoi polygons into eight groups $G_1 - G_8$ according to the values of the shape factor ζ [Eq. (1)]. For the densities corresponding to the packings obtained in the experiment, the distribution of ζ diminishes above ≈ 1.30 .

Group	Range	Color
G_1	$\zeta < 1.108$	yellow
G_2	$1.108 < \zeta < 1.125$	magenta
G_3	$1.125 < \zeta < 1.130$	cyan
G_4	$1.130 < \zeta < 1.135$	red
G_5	$1.135 < \zeta < 1.140$	green
G_6	$1.140 < \zeta < 1.160$	blue
G_7	$1.160 < \zeta < 1.250$	white
G_8	$1.250 < \zeta$	black

The shape factor is able to identify the occurrence of different domains in experimentally obtained packings of particles. Every domain is made up of the grains whose Voronoi polygons have similar values of the shape factor. We calculate a shape factor for each Voronoi cell, except for the opened cells located on the boundaries, which have incorrectly defined volumes. In order to clearly distinguish the domains made up of different Voronoi polygons, in Table II we classify the polygons according to their ζ values into eight groups $G_1 - G_8$. Group G_1 comprises near-regular hexagons, while other groups include less regular figures. To differentiate polygons belonging to different groups $G_1 - G_8$ we use the color coding in accordance with the definitions given in Table II. This allows us to easily distinguish the local arrangements of grains for the obtained packings.

In Fig. 7 we show the Voronoi tessellation of packings formed in the experiment with the beads of mass m_1 in various aqueous solutions of ZnCl_2 . Diagrams correspond to the fluid densities ρ_0 of 1.7 [Fig. 7(a)], 1.6 [Fig. 7(b)], 1.5 [Fig. 7(c)], 1.4 [Fig. 7(d)], and 1.3 g/cm^3 [Fig. 7(e)]. In Fig. 7(a) we observe a mixture of various Voronoi polygons. It is obvious that figures belonging to class G_7 dominates, where G_7 polygons are mostly distorted pentagons and hexagons. Only small islands of near-regular hexagons belonging to class G_1 are found. Moreover, small domains made up of $G_2 - G_6$ polygons can also be detected. This means that the beads are distributed quite randomly and no specific configurations of beads are formed.

As the density of fluid decreases further [Figs. 7(b) and 7(c)], more regular cells can be observed and their occurrence starts prevailing, though the structure of the system is still disordered. In the case of larger value of effective gravity [Fig. 7(d)] we find large domains made up predominantly of more or less regular hexagons (figures belonging to classes G_1 and G_2). One salient feature of Figs. 7(c) and 7(d) is the fact that grains spontaneously tend to form ordered hexagonal patterns. Orientation of the clusters of near-regular Voronoi cells observed in the bulk is not always parallel to the walls, suggesting that the order is not only wall induced, but nucleates and grows in the bulk. At first, such local organization is limited to short distances yielding an overall disordered packing. These clusters grow with a further increase of the effective gravity [Fig. 7(e)], so that grains end up in configurations where large clusters of near-regular Voronoi cells (class G_1) are found. These blocks are clearly separated by thin disordered regions made up of Voronoi polygons belonging to the class of more distorted Voronoi cells ($G_2 - G_7$). It must be stressed that tendency toward a crystalline order is much less pronounced in three dimensions than it is in two [35]. Indeed, in two dimensions the densest possible local configuration (hexagonal pattern) can be repeated infinitely in space. However, in three dimensions the closest attainable local configuration in a system of equal spheres is not compatible with translational symmetry and therefore it cannot be repeated in space without leaving gaps. After packing 12 spheres around the central one, with centers on the vertices of a regular icosahedron, there is a significant amount of free space left, although not enough to fit the thirteenth sphere. Such a compact local icosahedral configuration is geometrically frustrated and therefore it can be regarded as a source of structural heterogeneity.

To further quantify the structural changes in the packings of grains presented above, here we consider the probability distribution $P(\zeta)$ of the shape factor ζ [it is normalized to unity, i.e., $\int_0^\infty d\zeta P(\zeta) = 1$]. Figure 8 compares the probability distribution $P(\zeta)$ for the packings formed in solutions (A)–(E) (see Table I). For low intensities of the effective gravity $g_{\text{eff}}^{(1)}/g$, the Voronoi diagrams show a lot of cells with irregular rectangular, pentagonal or hexagonal structure [see Figs. 7(a) and 7(b)], and we thus get a broad distribution $P(\zeta)$ with no distinct maxima (Fig. 8). As the effective gravity $g_{\text{eff}}^{(1)}/g$ increases, the distribution $P(\zeta)$ becomes narrower and more

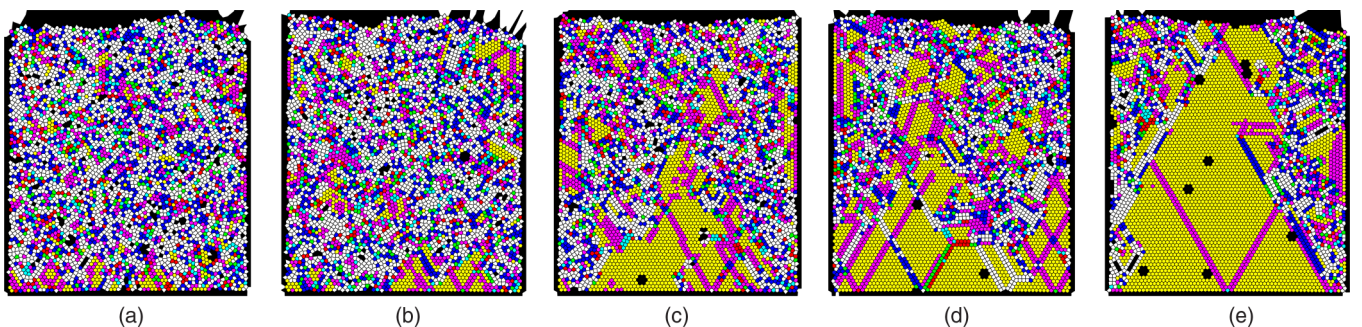


FIG. 7. (Color online) Voronoi diagrams of packings formed in various aqueous solutions of ZnCl_2 . Diagrams correspond to the fluid densities ρ_0 of (a) 1.7, (b) 1.6, (c) 1.5, (d) 1.4, and (e) 1.3 g/cm^3 . Voronoi cells are colored according to their shape factor ζ [Eq. (1)]. Color coding of the Voronoi polygons is defined in Table II. These results refer to the beads of mass $m_1 = 0.20 \text{ g}$.

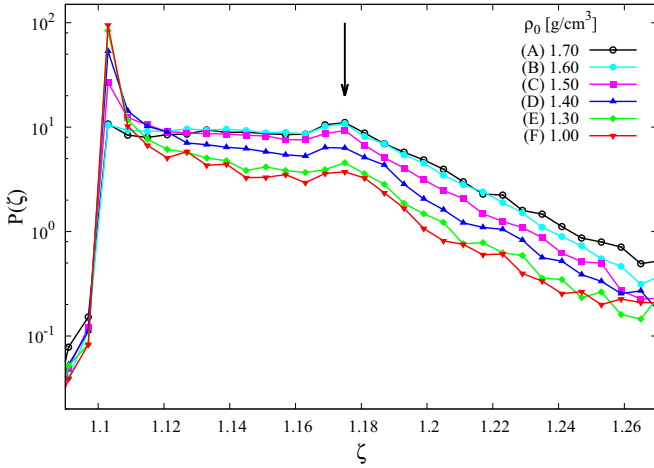


FIG. 8. (Color online) Probability distribution $P(\zeta)$ of the shape factor ζ for the packings formed in aqueous solutions (A)–(F) of ZnCl_2 (see Table I). The vertical arrow, centered at $\zeta \approx 1.175$, indicates the broad peak, which is composed primarily of overlapping contributions from distorted pentagons and hexagons.

localized around the lowest values of the shape factor (for a regular hexagon, $\zeta = 6/\sqrt{3\pi^2} \approx 1.103$). This behavior of the probability distribution $P(\zeta)$ corresponds to the decrease of the fraction of Voronoi polygons belonging to classes $G_5 - G_7$ (less circular cells). Furthermore, broad maximum in $P(\zeta)$, centered at $\zeta \approx 1.175$ is caused by overlapping contribution of distorted hexagons and pentagons. Indeed, the peak at $\zeta \approx 1.175$ vanishes if the pentagons and very distorted hexagons are not included in the computation of the distribution $P(\zeta)$. Examining snapshots (see, e.g., Fig. 7) shows that these distorted cells mainly come from the grains located in regions between solidlike domains.

Figure 9 compares the probability distributions $P(\zeta)$ for two packings formed under conditions that provide the same effective gravity, but different viscosity of the surrounding fluid. Experimental results for the distribution $P(\zeta)$ of the shape factor ζ are given for the packings of beads of mass $m_1 = 0.20$ g and $m_2 = 0.12$ g, which are created in the solution of type (A) and water, respectively. Solution (A) is 6.5 times more viscous than water, but the values of the corresponding effective gravities $g_{\text{eff}}^{(1)}/g = 5.57 \times 10^{-2}$ and $g_{\text{eff}}^{(2)}/g = 5.75 \times 10^{-2}$ are close to each other. In addition, the inset in Fig. 9 shows a plot of the radial distribution function $g(r)$ for these two packings. As seen in the inset, the major changes in the viscosity achieved in the experiment do not lead to important differences in the radial distribution function $g(r)$. Interestingly, we find that the microstructural properties for these two granular packings are very similar. This result is plausible for the following reasons. The possible effects of viscous drag on the grains are determined by measuring the velocity of particles during the settling. The resulting terminal velocity of a grain in a free fall through the liquid of maximum viscosity [solution of type (A)] is observed to be approximately $V_t = 10.5d_s s^{-1}$. At this measured velocity, the Reynolds number $\text{Re} = \rho_0 V_t d_s / \eta$ is about 98.5. The drag force exerted on the spherical particle of diameter d_s moving at a constant velocity V_t in a viscous fluid can be written generally

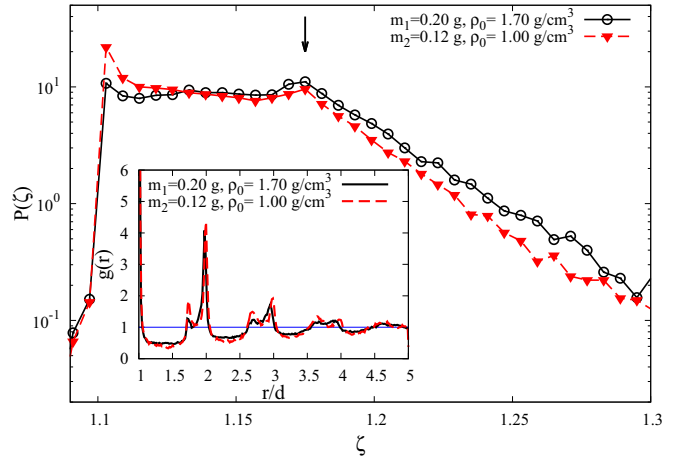


FIG. 9. (Color online) Results for the probability distribution $P(\zeta)$ of the shape factor ζ for two packings formed under conditions that provide the same effective gravity, but different viscosity of the surrounding fluid. Distributions $P(\zeta)$ are given for the packings created in the solution of type (A) (circles) and water (triangles), with beads of mass $m_1 = 0.20$ g and $m_2 = 0.12$ g, respectively. The corresponding values of the effective gravity are $g_{\text{eff}}^{(1)}/g = 5.57 \times 10^{-2}$ and $g_{\text{eff}}^{(2)}/g = 5.75 \times 10^{-2}$. The vertical arrow indicates the same peak as in Fig. 8. The inset shows the variation of the radial distribution function $g(r)$ for these two packings.

as:

$$F_v = \frac{1}{8} \rho_0 d_s^2 \pi C_D V_t^2, \quad (2)$$

where ρ_0 is the fluid density and C_d is the drag coefficient. The so called standard drag curve (SDC) for solid spheres establishes a universal relationship between the drag coefficient C_D and the Reynolds number Re . Here we give expression proposed by Turton and Levenspiel [36]:

$$C_D = \frac{24}{\text{Re}} (1 + 0.173 \text{Re}^{0.657}) + \frac{0.413}{1 + 16300 \text{Re}^{-1.09}}. \quad (3)$$

Note that relation (3) is valid for Reynolds numbers up to about 10^5 . Consequently, the calculated viscous drag F_v on the grains would therefore be $< 111 \mu\text{N} \approx m_1 g_{\text{eff}} \ll m_1 g$ at maximal velocities V_t . During the settlement of the packing, the beads undergo inelastic collisions and propagate under the effective gravity and the fluid drag in between collision events. This sequence of binary collisions with geometrically decreasing space and time scales brings the system to the state where neighboring beads are very close to contact. Finally, solidification occurs because the beads lose all of their kinetic energy. The local densification is accompanied by the formation of complex patterns and structures (arches or bridges). They are responsible for the voids that determine the volume fraction and for the force distributions in granular materials [21]. In the final stage of forming the cooperative structures, grain velocities are considerably smaller than the terminal velocity V_t , and thus the viscous drag F_v [Eq. (2)] on a grain is only a small part of its apparent weight $m g_{\text{eff}}$. Consequently, influence of the viscous effects on the grain motion in the final stage of forming the multiparticle structures

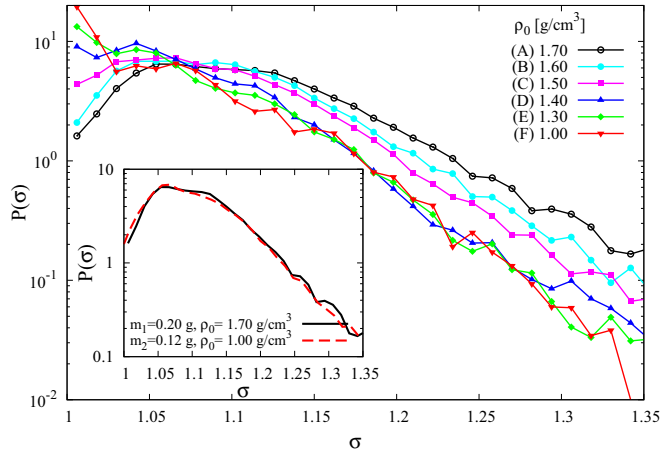


FIG. 10. (Color online) Probability distribution function $P(\sigma)$ of Voronoi areas σ normalized by the minimum area of a Voronoi cell, $\sigma_{\min} = \frac{\sqrt{3}}{2}d_s^2$. Distributions $P(\sigma)$ are given for the packings created in aqueous solutions (A)–(F) of ZnCl_2 (see Table I). The inset shows the distributions $P(\sigma)$ for the packings created in the solution of type (A) (solid) and water (dashed), with beads of mass $m_1 = 0.20$ g and $m_2 = 0.12$ g, respectively. The corresponding values of the effective gravity are $g_{\text{eff}}^{(1)}(A)/g = 5.57 \times 10^{-2}$ and $g_{\text{eff}}^{(2)}/g = 5.75 \times 10^{-2}$.

can be neglected, so that microstructural properties of the packing are predominantly determined by the effective gravity.

It is interesting to study the heterogeneity of the packings in more detail via the size σ of the Voronoi cell. In two dimensions, the minimum area of a Voronoi cell σ_{\min} is achieved for a hexagonal packing with $\sigma_{\min} = \frac{\sqrt{3}}{2}d_s^2$, where d_s is the diameter of a particle. The probability distribution $P(\sigma)$ of the Voronoi areas σ is defined as the probability of finding a polygon with area σ in the set of the Voronoi cells. It is normalized to unity, namely, $\int_{\sigma_{\min}}^{\infty} d\sigma P(\sigma) = 1$. We have calculated $P(\sigma)$ for various final packings and plotted it in Fig. 10 as a function of the area σ normalized by the minimum area of a Voronoi cell σ_{\min} . Distribution of Voronoi areas $P(\sigma)$ in two dimensions describes the deviation of a given structure from a hexagonal packing. In the case of perfect crystalline packing the Voronoi cell corresponding to each particle is a regular hexagon and thus $P(\sigma)$ becomes a δ function. For random particle structures, distribution $P(\sigma)$ broadens so that width of the distribution can be interpreted as the heterogeneity of a packing. From Figs. 7(a)–7(e) large variations in the sizes and shapes of the cells are noticeable at low values of the effective gravity $g_{\text{eff}}^{(1)}$, but less so as the $g_{\text{eff}}^{(1)}$ is increased reflecting the changes in the void spaces between grains. Consequently, distributions found for the packings formed in solutions (D), (E), and (F) are narrower in comparison to the packings in dense solutions (A), (B), or (C). One can see that $P(\sigma)$ broadens with decreasing value of the effective gravity $g_{\text{eff}}^{(1)}$ indicating that larger fluctuations in Voronoi areas are found with increasing heterogeneity. In addition, the inset in Fig. 10 shows the distribution $P(\sigma)$ for the two packings formed under conditions that provide the same effective gravity, but different viscosity of the surrounding fluid. Again, this result confirms that heterogeneity of the packings is predominantly determined by the effective gravity.

IV. CONCLUSIONS

In this paper, we have reported some experimental results concerning the microstructural properties of packings immersed in a liquid whose density could be varied. The packings have been generated under the chosen apparent gravity so that our results gain some insight into the properties of granular materials in a reduced gravity environment.

To examine the short scale structure in the packings, we evaluated the radial correlation function $g(r)$, which measures the particle density-density correlation at distance r for various intensities of the effective gravity $g_{\text{eff}}^{(1)}/g$. We found the expected changes in the behavior of the correlation function $g(r)$ with increasing the intensity of the $g_{\text{eff}}^{(1)}/g$. Namely, the oscillation of $g(r)$ quickly decays for the lowest values of $g_{\text{eff}}^{(1)}/g$, which means that long-range order does not exist in the system. As the effective gravity $g_{\text{eff}}^{(1)}/g$ is increased, the relative height of the secondary peaks increase, that is consistent with the increase in size of the compact clusters (see, e.g., Fig. 7). In addition, observed changes of connectivity numbers $\langle N_c^{(p)} \rangle$, ($p = 1, \dots, 6$) with $g_{\text{eff}}^{(1)}/g$ have provided an additional insight into the growth of hexagonal domains and formation of cooperative structures, such as arches or bridges (arching is directly related to the reduction of particle-particle contacts).

The organization of grains at local level was studied by analyzing the shape factor ζ [Eq. (1)], which is a quantifier of the circularity of the Voronoi cells associated with the individual particles. This gives a clear physical picture of the competition between less and more ordered domains of particles in the packing. For low intensities of the effective gravity the beads are distributed quite randomly and no specific configurations of beads are formed. In the case of larger value of the effective gravity we found that beads tend to organize themselves locally into ordered hexagonal patterns. Consequently, the narrowing of distribution $P(\zeta)$ that occurs with increasing of the effective gravity corresponds to the increase of the fraction of near-regular Voronoi cells.

Reorganization of the grains has also been analyzed through the distribution of pore volumes. This distribution is sensitive to small structural changes of the system. Delaunay free volumes have a distribution with a long tail, which progressively reduces while the apparent gravity increases. Furthermore, unlike in the three-dimensional case, these distributions have two peaks, which clearly indicate existence of local configurations with hexagonal and quadratic symmetry. Further, we have found that distribution of the Voronoi areas $P(\sigma)$ broadens with decreasing value of the effective gravity. Broadening in the distribution $P(\sigma)$ means that there is a broader distribution in the nearest-neighbor distances and therefore larger differences in the density fluctuations.

ACKNOWLEDGMENTS

This work was supported by the Ministry of Education, Science and Technological Development of the Republic of Serbia, under Grants No. ON171017, and No. III45016.

- [1] S. Torquato and F. H. Stillinger, *Rev. Mod. Phys.* **82**, 2633 (2010).
- [2] G. Parisi and F. Zamponi, *Rev. Mod. Phys.* **82**, 789 (2010).
- [3] R. Kurita and E. R. Weeks, *Phys. Rev. E* **82**, 011403 (2010).
- [4] J. D. Bernal and J. Mason, *Nature (London)* **188**, 910 (1960).
- [5] J. D. Bernal, *Proc. R. Soc. London, Ser. A* **280**, 299 (1964).
- [6] T. Aste, *J. Phys.: Condens. Matter* **17**, S2361 (2005).
- [7] T. Aste, M. Saadatfar, and T. J. Senden, *Phys. Rev. E* **71**, 061302 (2005).
- [8] S. Slotterback, M. Toiya, L. Goff, J. F. Douglas, and W. Losert, *Phys. Rev. Lett.* **101**, 258001 (2008).
- [9] N. Jain, D. V. Khakhar, R. M. Lueptow, and J. M. Ottino, *Phys. Rev. Lett.* **86**, 3771 (2001).
- [10] T. Arndt, T. Siegmann-Hegerfeld, S. J. Fiedor, J. M. Ottino, and R. M. Lueptow, *Phys. Rev. E* **71**, 011306 (2005).
- [11] T. Finger, A. Voigt, J. Stadler, H. G. Niessen, L. Naji, and R. Stannarius, *Phys. Rev. E* **74**, 031312 (2006).
- [12] T. Finger and R. Stannarius, *Phys. Rev. E* **75**, 031308 (2007).
- [13] C. C. Liao, S. S. Hsiau, and K. To, *Phys. Rev. E* **82**, 010302 (2010).
- [14] G. Y. Onoda and E. G. Liniger, *Phys. Rev. Lett.* **64**, 2727 (1990).
- [15] D. J. Costantino, J. Bartell, K. Scheidler, and P. Schiffer, *Phys. Rev. E* **83**, 011305 (2011).
- [16] F. Moučka and I. Nezbeda, *Phys. Rev. Lett.* **94**, 040601 (2005).
- [17] P. M. Reis, R. A. Ingale, and M. D. Shattuck, *Phys. Rev. Lett.* **96**, 258001 (2006).
- [18] I. Schenker, F. T. Filser, L. J. Gauckler, T. Aste, and H. J. Herrmann, *Phys. Rev. E* **80**, 021302 (2009).
- [19] T. Boutreux and P. G. de Gennes, *Physica A* **244**, 59 (1997).
- [20] T. Aste, *Phys. Rev. Lett.* **96**, 018002 (2006).
- [21] A. Mehta, G. C. Barker, and J. M. Luck, *J. Stat. Mech.: Theor. Exp.* (2004) P10014.
- [22] A. Ferguson and B. Chakraborty, *Phys. Rev. E* **73**, 011303 (2006).
- [23] S. Miller and S. Luding, *Phys. Rev. E* **69**, 031305 (2004).
- [24] L. A. Pugnaloni and G. C. Barker, *Physica A* **337**, 428 (2004).
- [25] L. A. Pugnaloni, M. G. Valluzzi, and L. G. Valluzzi, *Phys. Rev. E* **73**, 051302 (2006).
- [26] B. Drew, “Hough transform”, From MathWorld-A Wolfram Web Resource, created by Eric W. Weisstein. <http://mathworld.wolfram.com/HoughTransform.html>.
- [27] T. M. Truskett, S. Torquato, S. Sastry, P. G. Debenedetti, and F. H. Stillinger, *Phys. Rev. E* **58**, 3083 (1998).
- [28] J. L. Finney, *Nature (London)* **266**, 309 (1977).
- [29] R. Y. Yang, R. P. Zou, and A. B. Yu, *Phys. Rev. E* **62**, 3900 (2000).
- [30] A. R. Kansal, S. Torquato, and F. H. Stillinger, *Phys. Rev. E* **66**, 041109 (2002).
- [31] C. B. Barber, D. P. Dobkin, and H. Huhdanpaa, *ACM Trans. Math. Softw.* **22**, 469 (1996).
- [32] P. Philippe and D. Bideau, *Phys. Rev. E* **63**, 051304 (2001).
- [33] P. Richard, P. Philippe, F. Barbe, S. Bourles, X. Thibault, and D. Bideau, *Phys. Rev. E* **68**, 020301(R) (2003).
- [34] P. Richard, J. P. Troadec, L. Oger, and A. Gervois, *Phys. Rev. E* **63**, 062401 (2001).
- [35] G. Lumay and N. Vandewalle, *Phys. Rev. Lett.* **95**, 028002 (2005).
- [36] R. Turton and O. Levenspiel, *Powder Technol.* **47**, 83 (1986).
- [37] M. Laliberté, *J. Chem. Eng. Data* **52**, 321 (2007).